Passive UHF RFID-based Knitted Wearable Compression Sensor

Md Abu Saleh Tajin, *Student Member, IEEE*, Chelsea E. Amanatides, Genevieve Dion, and Kapil R. Dandekar, *Senior Member, IEEE*

Abstract-One of the major challenges faced by passive onbody wireless Internet of Things (IoT) sensors is the absorption of radiated power by tissues in the human body. We present a battery-less, wearable knitted Ultra High Frequency (UHF, 902-928 MHz) Radio Frequency Identification (RFID) compression sensor (Bellypatch) antenna and show its applicability as an on-body respiratory monitor. The antenna radiation efficiency is satisfactory in both free-space and on-body operations. We extract RF (Radio Frequency) sheet resistance values of three knitted silver-coated nylon fabric candidates at 913 MHz. The best type of fabric is selected based on the extracted RF sheet resistance. Simulated and measured performance of the antenna confirm suitability for on-body applications. The proposed Bellypatch antenna is used to measure the breathing activity of a programmable infant patient emulator mannequin (SimBaby) and a human subject. The antenna is highly sensitive to respiratory compression and relaxation. Fluctuations in the backscatter power level/Received Signal Strength Indicator (RSSI) in both cases range from 6 dB to 15 dB. The improved on-body read range of the proposed sensor antenna is 5.8 m, about 10 times higher than its predecessor wearable knitted strain sensing Bellyband antenna (0.6 m). The maximum simulated Specific Absorption Rate (SAR) on a human torso model is 0.25 W/kg, lower than the maximum allowable limit of 1.6 W/kg.

Index Terms—Biomedical sensor, compression sensor, Internet of Things (IoT), knitted conductive fabric, on-body antenna, respiration sensor, Radio Frequency (RF) sheet resistance, Radio Frequency Identification (RFID), silver-coated nylon, Ultra High Frequency (UHF), wearable textile antenna

I. INTRODUCTION

Commercial Radio Frequency Identification (RFID) tags are largely used in diverse applications including inventory and warehouse management, transportation, localization, agriculture, access control, libraries, and museums. Passive RFID tags harvest wireless energy radiated by an external reader antenna, and they do not require batteries. As a result, passive tags are lightweight and do not demand meticulous maintenance, which opens the doors to fascinating applications in IoT-based healthcare systems. However, body-worn tags must be carefully designed to account for the potentially limiting

This research is supported by the National Science Foundation under Grant CNS-1816387 and the National Institutes of Health under Grant R01 EB029364. Any opinion, findings, and conclusion or recommendations expressed in this materials are those of the author(s) and do not necessarily reflect the views of the National Science Foundation or the National Institutes of Health

M. A. S. Tajin and K. R. Dandekar are with the Department of Electrical and Computer Engineering, Drexel University, Philadelphia, PA 19104 USA (email: mt3223@drexel.edu; dandekar@drexel.edu).

C. E. Amanatides and G. Dion are with the Center for Functional Fabrics, Drexel University, Philadelphia, PA 19104 USA (email:cek56@drexel.edu; gd63@drexel.edu).

effects of human body tissue-induced dielectric loss. The majority of commercial Ultra High Frequency (UHF) passive RFID tags are meandered dipole antennas with small chips [1]. Those tags are made from thin metal sheets and are not necessarily designed for on-body applications, where usercomfort and flexibility are matters of concern. The introduction of knitted conductive yarn-based wearable tags [2, 3] has been successful in ensuring comfort for the users. However, those tags are different subcategories of dipole antennas. In general, they have omnidirectional radiation patterns in free space. Average relative permittivity (or dielectric constant) of human body tissue (ϵ_{body}) is 50 (source: HFSS - High Frequency Structure Simulator) (compared to ϵ_{air} = 1) and dielectric loss tangent 0.5. When placed on a human subject for sensing purposes, most of the radiation is absorbed by the human body tissues in the form of dielectric loss. The read range of the system is drastically reduced as a result. For example, our previous work, the Bellyband antenna [3] has on-body read range 0.6 m [4]. Additionally, the weaker signal from the antenna to the reader incurs the detrimental effects of noise. To alleviate the aforementioned issues, we propose a compression sensor, instead of a strain sensor, for respiratory monitoring applications. The proposed sensor/antenna can be used for other compression sensing applications as well.

Bellyband antenna-based sensing is a combination of antenna tuning-detuning and radiation efficiency fluctuation due to successive stretch and relaxation. Body tissue composition varies from person to person. Consequently, antenna tuningbased sensing is prone to variability. Some modern UHF RFID chips offer automatic tuning control to facilitate the use of tags in dynamic environments. In other words, the RFID chip changes its input impedance based on the impedance of the antenna, to ensure maximum possible power transfer. For example, the Monza R6 chip [5] provides this functionality through a feature called "autotune" [6]. The proposed compression sensor is a differential-fed patch structure. The top and ground layers are combinations of knitted conductive fabric and nonconductive fabrics. In the middle, there is a compressible substrate made from polyethylene foam. A Monza R6 chip is placed on the top layer using a printed circuit board (PCB) inserted into a knitted heat shrink pocket, connecting the two radio frequency (RF) pads of the chip to the top antenna patches. The PCB and pocket are specifically designed to facilitate inductive coupling without any soldering required. The PCB provides a larger surface area for the conductive yarns to come in contact with, allowing for electrical connection to the Monza R6 chip. The pocket for the PCB is knit with

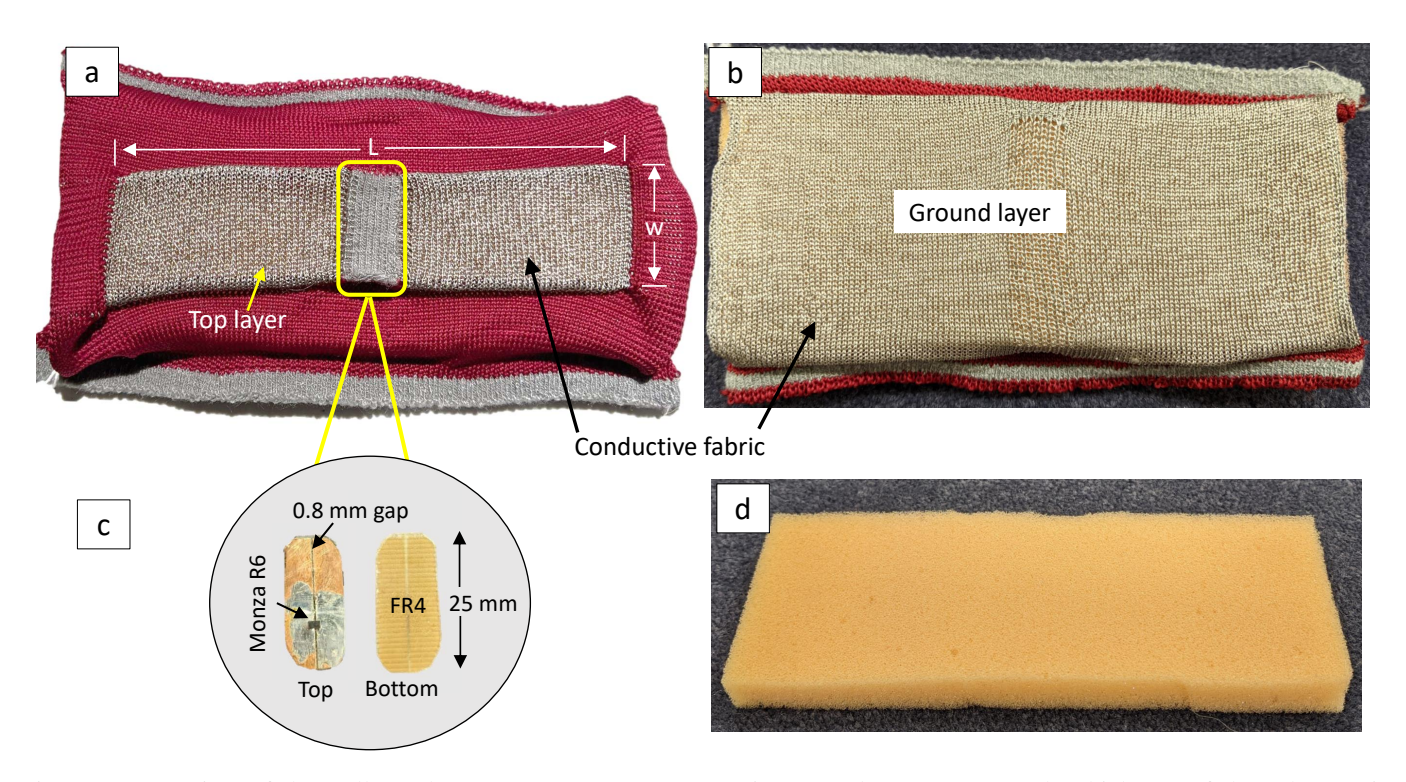


Fig. 1: a) Top view of the Bellypatch antenna prototype. L = 135 mm, and w = 30 mm. The thickness of the substrate in between the top and ground layers is 11 mm, b) Bottom view, c) FR4 PCB with Monza R6 chip, d) Flexible substrate.

an elasticated varn that further shrinks upon heat treatment and prevents the pocket from stretching. Since the conductive yarns overlap into the pocket section and are stabilized in place by the heat setting process, the connection between the conductive yarns and the PCB is stabilized. Knitting provides advantages over other textile manufacturing processes. Specifically, the non-conductive fabric, conductive fabric, and PCB pocket are seamlessly produced and integrated in a single process on a CNC knitting machine. Ultimately, to facilitate commercialization of the proposed technology, PCB placement could also be automated and integrated into this manufacturing process. The radiation efficiency of the proposed Bellypatch antenna is a strong function of the substrate height (h). As a result, the backscattered power levels and Received Signal Strength Indicator (RSSI) at low-h states are lower compared to high-h states. As the diaphragm of the user repeatedly compresses and relaxes the antenna, the RSSI at the reader end fluctuates, leading to compression sensing capability. Although the input impedance of the antenna fluctuates due to the variation in substrate height, the 'autotune' feature of the chip dynamically compensates for its effects. In addition, the intrinsic/free-space radiation pattern of the proposed antenna is directional. As a result, the antenna performance is minimally affected by the proximity of the human body. The maximum tested read range of one of the variants (145 mm length) of the proposed Bellypatch antenna is 5.8 m. Compared to the previous Bellyband antenna (0.6 m range), the new Bellypatch antenna read range is almost 10 times higher. The improved read range is partially due to the lower wake-up power of the Monza R6 chip [5] compared to the Murata MAGICSTRAP [7]. However, the proposed Bellypatch antenna also shows superior on-body radiation efficiency. In a later section, we will show that if the Bellyband is fabricated with a Monza R6 chip, the read range of the Bellypatch will still be 3.5-times higher.

In addition to extended read range, RSSI swings are deeper and easily recognizable which provides a good dynamic range when this quantity is being used for sensing applications.

RF structures and antennas fabricated with conventional metals can be directly simulated using electromagnetic simulators since they have fixed conductivity values. In comparison, knitted conductive yarns and fabrics show variability in conductivity performance based on a number of internal and external factors, e.g., knitting pattern, coating thickness, coating material, oxidation, moisture, sweat [8], knitting and handling, etc. We fabricated transmission line samples with metal ground layers, FR4 substrates, and the top layer made with knitted conductive fabric samples. We employ a new technique (that we developed [8]) for the extraction of RF sheet resistance values of different samples. Based on the sheet resistance values, an optimum knitted conductive fabric is selected. Knitted conductive fabrics are designed in High Frequency Structure Simulator (HFSS), and the extracted sheet impedance value is applied to perform simulations.

II. RELATED WORK

Patch antenna-based sensors have been proposed for strain and structural crack monitoring applications [9, 10]. Applied strain or increased crack size deforms the patch antenna size, causing a shift in the resonant frequency. Occhiuzzi *et al.* developed a passive RFID strain sensor using a meandered dipole antenna [11] for monitoring the structural health of

damaged structures and vehicles. Merilampi *et al.* fabricated an RFID strain sensor by screen printing silver ink conductors on stretchable polyvinyl chloride and fabric substrates [12]. A combination of non-stretchable and stretchable fabric has been used for strain monitoring [13].

Conformal patch antennas have been proposed for metal-mounting [14, 15] as well as on-body tracking applications [16, 17]. Sohrab *et al.* proposed a patch antenna [18] that is robust to metal and non-metal host materials. However, the conductive parts of these antennas are made mostly with copper, and their substrates are rigid as well. Rigid antennas are not comfortable to wear on-body; hence it is challenging to use them for on-body applications.

Patron et. al [2] proposed a wearable passive RFID strain sensor made from knitted conductive and non-conductive yarns. The conductive yarns are made from silver-coated nylon threads. The antenna is a differential-feed folded dipole structure, and the UHF RFID chip is inductively coupled with the antenna ports. Liu et. al improved the design [3] by soldering the RFID chip on top of a small and thin copper PCB and inserting it into a pocket knitted into the fabric antenna. These two classes of antennas are called "Bellyband". Between successive stretch and relaxation, antenna radiation efficiency and the tuning between the RFID chip and the flexible antenna changes, leading to different levels of backscatter power or RSSI at the reader end. The battery-less Bellyband antenna can be used for wireless monitoring of infant respiration, uterine contraction in pregnant women, and body movements. Bellyband offers very good user-comfort and flexibility. However, the on-body read range is very low (0.6 m) [4]. In addition to that, the FCC (Federal Communications Commission) requires that a minimum of 20 cm distance must be maintained between the reader antenna and the user [19]. Although the strain sensor has good performance for free-space applications, the on-body performance is very limited by reduced radiation efficiency due to power loss in the human body. The knitted "Bellypatch" antenna we propose builds a bridge between the rigid patch antennas and the wearable Bellyband antenna. Not only does it retain radiation efficiency while on-body, but it also works as a compression sensor by utilizing its compressible substrate layer. To the best of our knowledge, this is the first knitted conducive yarn-based passive UHF RFID compression sensor.

In addition to strain and compression sensing, in recent years, wearable UHF RFID sensors are being developed for a wide range of applications. However, there exists a gap between research laboratories and commercialization that needs to be filled [20]. Wearable UHF RFID-based wearable moisture [21, 22], temperature sensors [23] are being developed. The rapid development of 2D nanomaterials with multiple conductivity variants (*e. g.* MXene [24], graphene [25], *etc.*) and their integration into textile [26, 27] offer exciting potential in designing wearable sensors.

III. SIMULATION

Bellypatch is a differential patch antenna, comprised of knitted conductive and non-conductive fabrics, a compressible polyethylene substrate, and a passive UHF RFID Monza R6

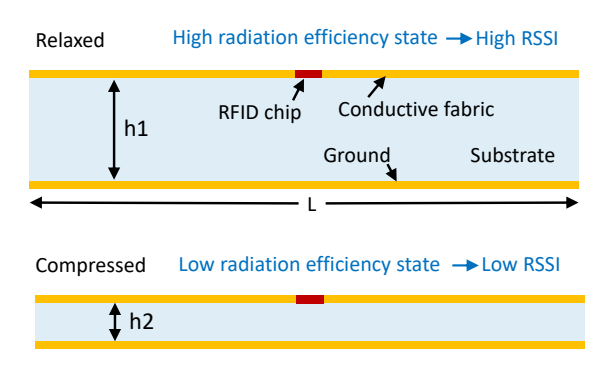


Fig. 2: Front view of the bellypatch antenna. In the relaxed state (h1), the antenna efficiency is higher compared to the compressed state (h2).

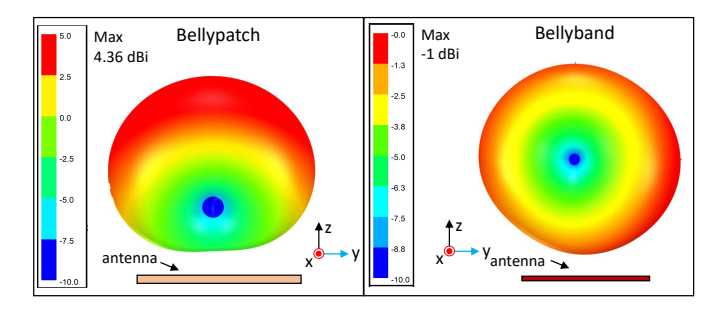


Fig. 3: Comparison of free-space 3D gain (dBi) pattern between the Bellypatch and the Bellyband [3] antenna. Bellyband has an omnidirectional radiation pattern, whereas the proposed Bellypatch has a directional radiation pattern.

chip [5]. The chip is soldered on a small PCB and the chip-PCB structure is inserted into a small pocket knitted in the middle region of the antenna top layer. The goal of the simulation process is to attain three important features - i) impedance match between the antenna and the chip, ii) good on-body radiation efficiency and iii) gain variability with substrate thickness. Knitted conductive fabrics are different than conventional metals. Their conductivity is dictated by a few factors, e.g. coating thickness, oxidation, moisture, sweat, knit pattern, knitting, handling, etc. [8]. Instead of using a perfect electric conductor surface, we define the knitted conductive fabric as an impedance type boundary in HFSS. In a later section, we will show the extraction procedure of sheet resistance. The sheet impedance value assigned to the knitted conductive fabric is $(0.3 + j2.5) \Omega/sq$. We choose 11 mm substrate height, 30 mm top layer width, and 0.8 mm separation between the two patches on the top. These values are chosen to have a sensor small enough for on-body applications with different age groups of users. We run a sweep on the top layer length (L) (Fig. 1) to find the optimum antenna size.

A. Impedance Match

Monza R6 chips (and almost all UHF RFID tags) are a balanced structure. In other words, the electrical signals

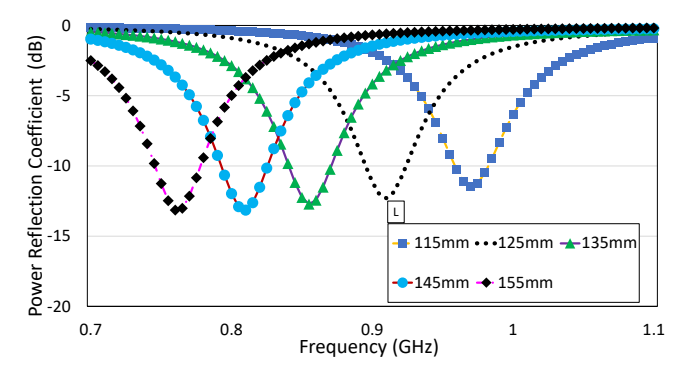


Fig. 4: Simulated power reflection coefficient (Γ) vs. frequency plot for different L (antenna top layer length) values of a flat Bellypatch antenna in free-space.

in the two pads of the chip are electrically 180° apart. If the antenna feeding system is unbalanced, a balanced to unbalanced (balun) transformer needs to be used. On the other hand, a balanced antenna structure can be directly connected to the chip pads.

The differential power reflection coefficient (Γ) is calculated using the following formula [2],

$$\Gamma = 20 \log_{10} \left(1 - \frac{4R_a R_c}{|Z_a + Z_c|^2} \right)$$
 (1)

where Z_a , Z_c , R_a , and R_c indicate the antenna impedance, chip impedance (12 - j120 Ω for Monza R6 at 915 MHz [5]), real part of the antenna impedance, and real part of the chip impedance. Fig. 4 shows the simulated power reflection coefficients (Γ) as L varies from 115 mm to 155 mm. From an antenna tuning point of view, 125 mm appears to be the best choice. However, antenna radiation efficiency also needs to be considered while choosing optimized antenna dimensions. Modern UHF RFID chips offer an adaptive impedance match feature to facilitate use in diverse environments. For example, the Monza R6 chip has an "autotune" feature [6] that automates the antenna-chip impedance match procedure. Because of this adaptive nature of the chip, we have greater flexibility in choosing antenna dimensions.

B. Radiation Efficiency

The dipole family of antennas has an omnidirectional radiation pattern in free space. However, when placed on a human subject, a large portion of the radiated energy is absorbed by the dielectric body tissues. As a result, the antenna radiation efficiency is significantly reduced [4]. This in turn limits the read range of the antenna/sensor. Fig. 5 shows simulated Bellypatch antenna radiation efficiency as a function of L. Radiation efficiency increases with an increase in L. The 155 mm antenna offers maximum radiation efficiency in the range. However, the antenna becomes bulky and would be cumbersome for applications with infants. We choose the 135 mm version as the primary design for further simulations and experiments. Fig. 6 shows the HFSS simulation of the antenna placed on a human torso model. The simulated on-body radiation efficiency of the antenna is 40.8%. As a result,

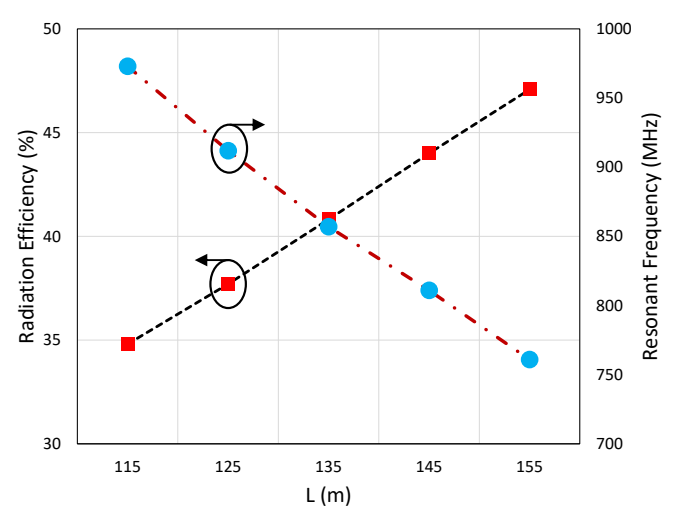


Fig. 5: Radiation efficiency and resonant frequency as a function of top layer length of the antenna (flat and in free-space).

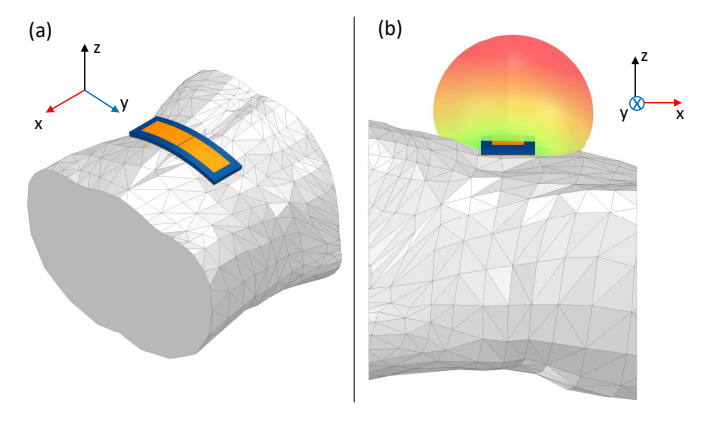


Fig. 6: a) Isometric view of the bellypatch antenna (135 mm \times 30 mm \times 11 mm) wrapped on a human torso model (voxel) in HFSS, b) Right-hand-side view of the on-body antenna with the directional 3D radiation pattern shown.

the proposed Bellypatch antenna shows good on-body antenna gain. On the other hand, the Bellyband antenna shows 2.8% on-body radiation efficiency, leading to poor antenna gain and limited read range. In Fig. 7, the on-body 2D radiation patterns of the Bellyband and the proposed Bellypatch antenna are juxtaposed for comparison. The maximum gain of the Bellyband antenna is -15.3 dBi, while the Bellypatch shows a 3.6 dBi maximum gain.

C. Gain Variability

The gain of the proposed compression sensing Bellypatch antenna is a strong function of substrate thickness. The antenna shows a higher gain at the relaxed state and a lower gain in compressed states. We sweep the substrate height (h) of the antenna on a human body model. Fig. 8 shows that the antenna gain is maximum (3.6 dBi) for h = 11 mm (highest). As h becomes lower, antenna gain gets reduced. Minimum gain (-7 dBi) is observed for h = 1mm (lowest). From this part of the

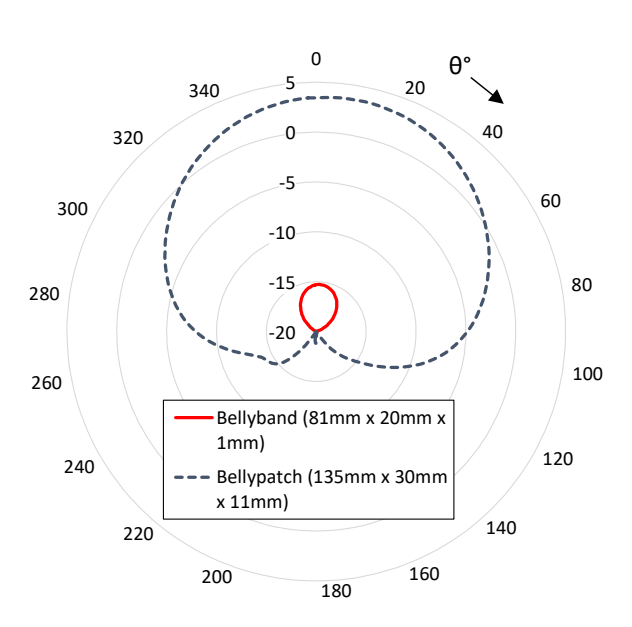


Fig. 7: Comparison of on-body 2D gain pattern between the Bellyband [3] and the Bellypatch (proposed) antennas. The Bellyband antenna (previous version) shows very low on-body gain (-15.3 dBi maximum), while the Bellypatch (proposed version) antenna has very good gain performance (3.6 dBi maximum) on-body. The radii of the plot indicate antenna gain in dBi.

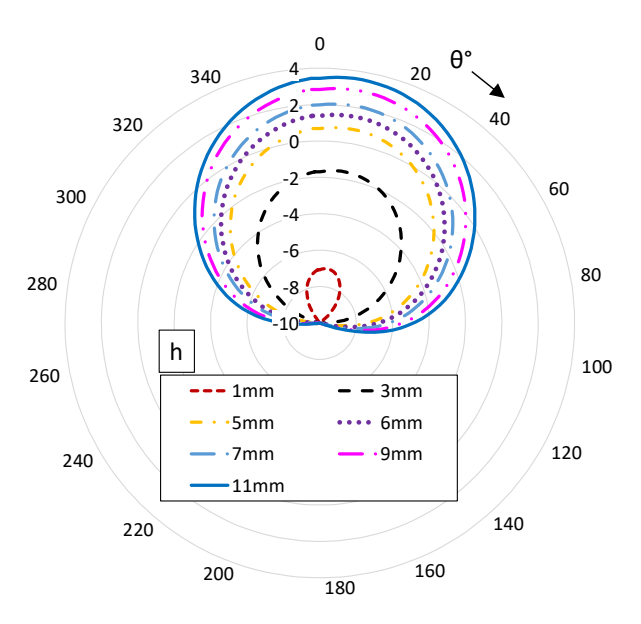


Fig. 8: The gain pattern of the Bellypatch antenna at different substrate thickness levels. The gain of the patch structure is low for thin substrate and vice-versa. The radii of the plot show gain in dBi.

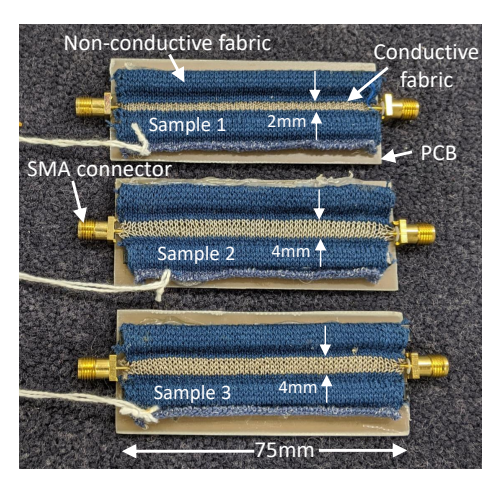


Fig. 9: Transmission line samples whose top layers are made with conductive fabric.

simulation, it is clear that the proposed wearable antenna is suitable for on-body compression sensing.

IV. SENSOR CONSTRUCTION

The sensor construction consists of a few steps: *i)* RFID chip selection, *ii)* selection of knitted conductive fabric, and *iii)* substrate material selection.

A. RFID Chip

We choose state-of-the-art Monza R6 [5] chips as the transponder on the sensor antenna. The chip has a lower sensitivity (minimum wake-up power) compared to earlier versions (e. g. Monza R2, R4, etc.). The chip has two differential RF input pads (RF+ & RF-) for an antenna. The size of the chip is $461.1\mu m \times 400\mu m$ [5].

B. Knitted Conductive Fabric

The knitted conductive fabric largely dictates the read range of the antenna. In other words, the ohmic losses in the top and ground layers play an important role in the antenna radiation efficiency. As a result, the antenna gain is affected, which in turn, partially governs the antenna read range. In a recent work [8] we have demonstrated a method of extracting ultra-high-frequency sheet resistance of knitted conductive from scattering parameter measurements of transmission lines. A rectangular knitted conductive fabric, supported by nonconductive fabric on both sides, is placed on a single-sided FR4-based board. Sub-miniature version A (SMA) connectors are attached on both sides of the conductive fabric. Following similar techniques, we construct three groups of microstrip transmission lines (Fig. 9). These three transmission line samples used the same pattern and number of stitches. However, a different yarn is used for each; sample-1 is made with silvercoated nylon yarns with an elastomeric core (2X 100/34), sample-2 is made with silver-coated nylon plied yarns (2X100-XS-34), and sample-3 is made with silver-coated nylon highbulk yarns (4 ends of 70 XS 34, plied with 100 twists per

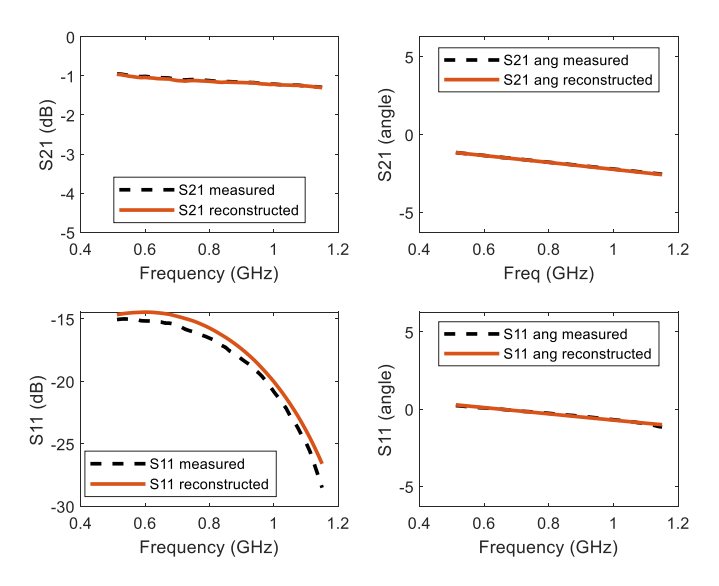


Fig. 10: Measured (measurement-plane-corrected) and reconstructed (from extracted RLGC parameters) scattering parameters of the sample-1 transmission line.

meter). All yarns are produced by Noble Biomaterials Inc (Scranton, PA, USA).

Transmission line samples and later, antennas are fabricated on a 14 gauge Shima Seiki industrial knitting machine (SVR122-SR). The yarn used for the fabric surrounding the conductive transmission lines is nylon and modal blend yarn (85% Modal/15% Nylon, Silk City Fibers, Paterson, NJ, USA). For the full antennas, the varn used for the surrounding, non-conductive fabric is a multi-filament polyester (1/150/50, American Silks, High Point, NC, USA). The two-layer antenna structure is produced using a custom knitting program, resulting in a double-layer fabric, with open ends for the insertion of the substrate material.

S-parameters $(s_{i,j}; i, j = 1, 2)$ of these two-port transmission lines are measured with a vector network analyzer (VNA). The true S-parameters of the device under test (DUT) are derived by separating the contribution of the connectors using the following equation,

$$[\mathbf{S}_{\text{Measured}}] = \begin{bmatrix} e^{-j\theta} & 0\\ 0 & e^{-j\theta} \end{bmatrix} \begin{bmatrix} S_{11} & S_{12}\\ S_{21} & S_{22} \end{bmatrix} \begin{bmatrix} e^{-j\theta} & 0\\ 0 & e^{-j\theta} \end{bmatrix}$$
(2)

where $\theta = \beta l_c$, β is the propagation phase constant, and l_c is the length of each connector. ABCD parameters are extracted from the measurement-plane-corrected S-parameters:

$$A = \frac{(1+s_{11})(1-s_{22}) + s_{12}s_{21}}{2s_{21}}$$
 (3a)

$$B = Z_0 \frac{(1+s_{11})(1+s_{22}) - s_{12}s_{21}}{2s_{21}}$$
 (3b)

$$A = \frac{(1+s_{11})(1-s_{22}) + s_{12}s_{21}}{2s_{21}}$$
(3a)

$$B = Z_0 \frac{(1+s_{11})(1+s_{22}) - s_{12}s_{21}}{2s_{21}}$$
(3b)

$$C = \frac{1}{Z_0} \frac{(1-s_{11})(1-s_{22}) - s_{12}s_{21}}{2s_{21}}$$
(3c)

$$D = \frac{(1-s_{11})(1+s_{22}) + s_{12}s_{21}}{2s_{21}}$$
(3d)

$$D = \frac{(1 - s_{11})(1 + s_{22}) + s_{12}s_{21}}{2s_{21}}$$
 (3d)

where Z_0 is the normalizing impedance (50 Ω). The extracted ABCD parameters are used to extract the characteristic

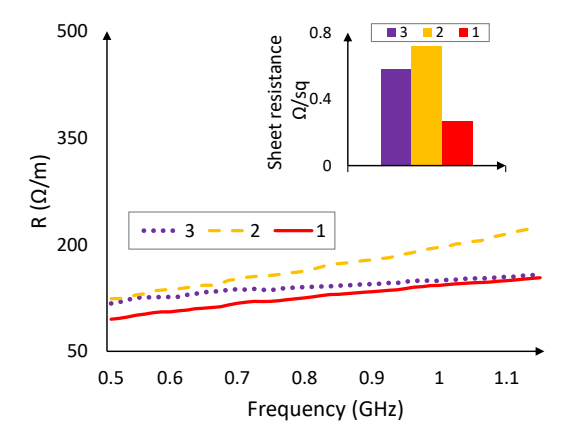


Fig. 11: Extracted R-parameter and sheet resistance from three transmission line samples.

impedance (Z_c) and propagation constant $(\gamma = \alpha + j\beta)$ of the transmission line:

$$Z_c = \sqrt{\frac{B}{C}} \; ; \quad \gamma = \frac{1}{l} \cosh^{-1}(A)$$
 (4)

where l is the length (74mm) of the transmission line. Since the extraction of RLGC parameters is an ill-posed mathematical problem, the direct extraction gives rise to unexpected values of R and G parameters. We accept γ and reconstruct Z_c by optimization. The per unit length distributed parameters can be found as:

$$R = Re(\gamma Z_c) \; ; \; L = Im(\gamma Z_c)/\omega$$
 (5a)

$$G = Re(\gamma/Z_c) \; ; \; C = Im(\gamma/Z_c)/\omega$$
 (5b)

where $\omega = 2\pi f$ (f is frequency in Hz) is the angular frequency. To validate the extracted parameters, S-parameters are reconstructed from the RLGC parameters [28, 29] (fig. 10),

$$\gamma = \sqrt{(R + j\omega L)(G + j\omega C)}$$
, $Z_c = \sqrt{\frac{R + j\omega L}{G + j\omega C}}$ (6a)

$$[\mathbf{S}_{\text{Rec}}] = \frac{1}{D_s} \begin{bmatrix} (Z_c^2 - Z_0^2) \sinh \gamma l & 2Z_c Z_0 \\ 2Z_c Z_0 & (Z_c^2 - Z_0^2) \sinh \gamma l \end{bmatrix}$$
(6b)

where $D_s = 2Z_cZ_0\cosh\gamma l + (Z_c^2 + Z_0^2)\sinh\gamma l$. We assumed the transmission line is symmetric and reciprocal $(S_{11} \equiv S_{22})$ and $S_{12} \equiv S_{21}$). The extracted R-parameter (equation 5) is then used to calculate the sheet resistance at our frequency of interest (913MHz). Fig. 11 shows the extracted R-parameters of the three transmission line groups depicted in fig. 9. The total conduction loss in the transmission line can be attributed to the top layer resistance (R_{fabric}), ground layer resistance (R_{gnd}) , and a fraction of radiation resistance (R_{rad}) .

$$R_{\text{total}} = \left(\frac{l}{1000}\right) R = R_{\text{fabric}} + R_{\text{gnd}} + R_{\text{rad}}$$
 (7)

In our previous work [8], we showed that the ground layer resistance, as well as the radiation resistance, are negligibly small compared to the top layer resistance. Hence, it is a

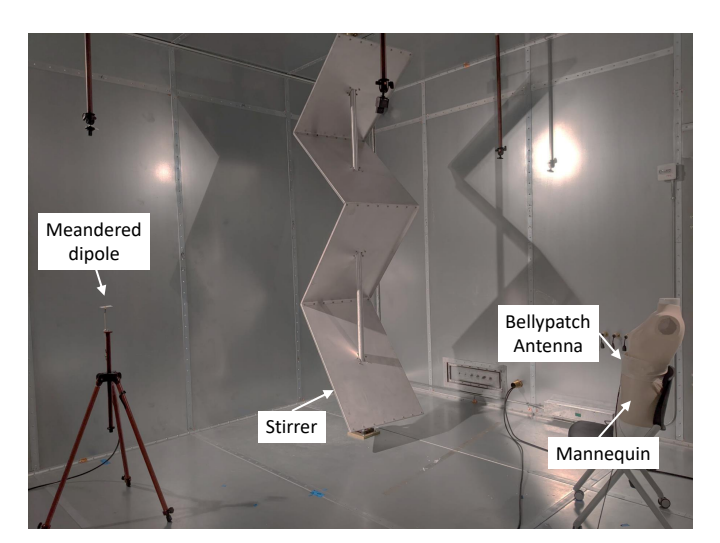


Fig. 12: Radiation efficiency measurement of the Bellypatch antenna in a reverberation chamber.

valid approximation that $R_{\rm fabric} \approx R_{\rm total}$. Sheet resistance $(R_s, \Omega/sq)$ of the conductive fabric is,

$$R_{\rm s} = \left(\frac{w}{l}\right) R_{\rm fabric} \tag{8}$$

where w is the width of the top layer of the transmission line. Fig. 11 shows the comparison of sheet resistance of three sample groups. We observe that sample-1 has significantly lower sheet resistance compared to the other two groups. This means ohmic losses will be minimum and radiation efficiency will be maximum if we construct our antenna with the group-1 conductive fabric. Based on the results of the transmission line samples, we pick the conductive yarn to move forward with the fabrication of the antenna.

C. Substrate Material

The deformation/compression of the substrate causes the fluctuation in RSSI. As a result, it is very important to choose a substrate that is easily compressible and comfortable to wear. The relative permittivity (ϵ_r) of the substrate material largely determines the antenna size. In general, fabric materials with higher dielectric constant tends to be less compressible. The antenna would be smaller in size, but with lower radiation efficiency. On the other hand, fabrics at the lower end of the relative permittivity list are more compressible. This physical feature comes at the cost of a larger antenna. However, the higher radiation efficiency and compressibility compensate for that with extended read range and sensitivity. We use polyethylene foam substrate with $\epsilon_r = 2.4$. The dimension of the substrate is 155 mm \times 50 mm \times 11 mm in the relaxed state.

V. ANTENNA MEASUREMENTS

A. Radiation Efficiency

We place a meandered dipole antenna and a standard dipole antenna (with known radiation efficiency) in a reverberation chamber equipped with a vertical stirrer (Fig. 12). After

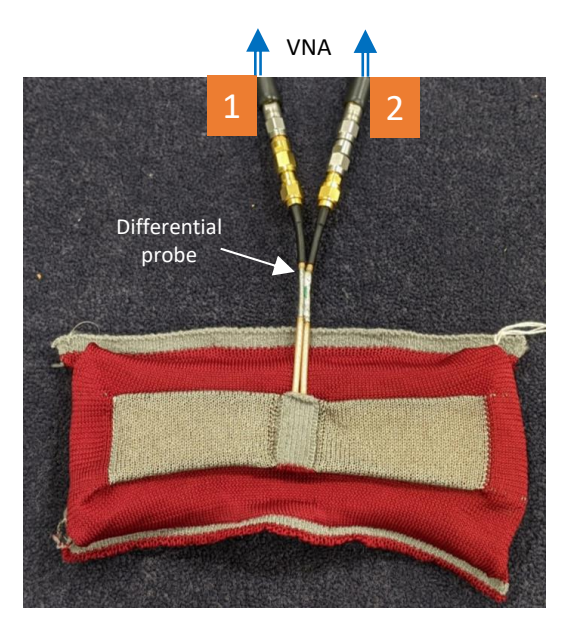


Fig. 13: Impedance measurement of the bellypatch antenna with differential coaxial cable and vector network analyzer (VNA).

recording 2-port s-parameters with an external Vector Network Analyzer (VNA) at different stirrer positions, the standard dipole antenna is replaced with the bellypatch antenna on a mannequin. We use a balun (balanced-to-unbalanced) converter in between the unbalanced coaxial cable (connected to one port of the VNA) and the balanced Bellypatch antenna ports. The radiation efficiency of the Bellypatch antenna is measured using the following equation [4],

$$\eta_{\text{AUT}}^{\text{rad}} = \frac{\left\langle \left| S_{21}^{\text{AUT}} \right|^2 \right\rangle}{\left\langle \left| S_{21}^{\text{SD}} \right|^2 \right\rangle} \frac{(1 - \left\langle \left| S_{11}^{\text{SD}} \right|^2 \right\rangle)(1 - \left\langle \left| S_{22}^{\text{SD}} \right|^2 \right\rangle)}{(1 - \left\langle \left| S_{11}^{\text{AUT}} \right|^2 \right\rangle)(1 - \left\langle \left| S_{22}^{\text{AUT}} \right|^2 \right\rangle)} \eta_{\text{SD}}^{\text{rad}}$$
(9)

where $\eta_{\rm SD}^{\rm rad}$, and $\eta_{\rm AUT}^{\rm rad}$ are the radiation efficiencies of the standard dipole and the Antenna Under Test (AUT) respectively. The sign $\langle \ \rangle$ is used to indicate the ensemble average. The superscript 'SD' indicates the first setup with the standard dipole and the meandered dipole, and 'AUT' indicates the second setup where the standard dipole is replaced by the AUT (Bellypatch).

B. Power Reflection Coefficient (Γ)

Since the proposed Bellypatch antenna has a differential feed, power reflection coefficient (Γ in Eq. 1) cannot be measured with a single unbalanced coaxial cable. Instead, we use a differential probe for measuring 2-port s-parameters and calculating the differential power reflection coefficient as a function of frequency. The outer metal shields of two short coaxial cables (\sim 130 mm in length) are soldered together so that they have a common RF ground. One end of the coaxial cables have SMA connectors that connect directly to the VNA ports, and the other end has open center connectors that are soldered to a PCB with two pads. The VNA is calibrated with the open-ended dielectric probe, before soldering with

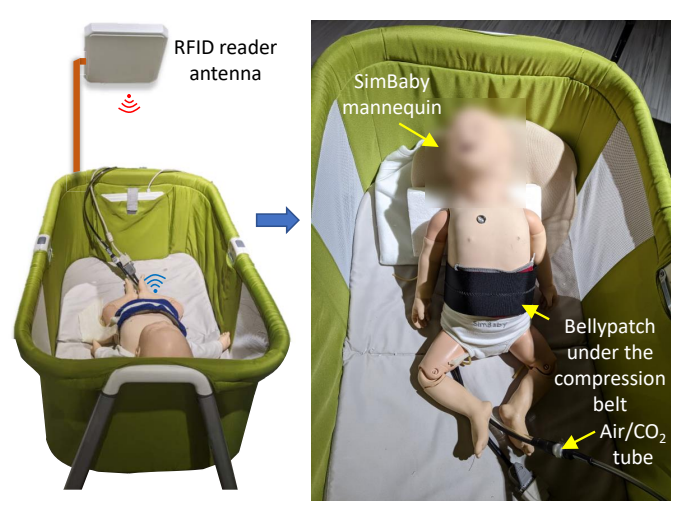


Fig. 14: SimBaby mannequin [33] in the crib with the wearable compression sensor (Bellypatch). The external compression belt (right) facilitates the compression process.

the PCB, as a usual 2-port setup. The PCB is inserted into the pocket of the Bellypatch. As a result, currents through the externally conjoint coaxial cables (differential probe) flow separately into the two top-layer patches. Fig. 13 shows the setup for measuring S-parameters with the differential probe. The differential input impedance of the Bellypatch can be found from the measured S-parameters [2]:

$$Z_{\rm a} = R_{\rm a} + jX_{\rm a} = 2Z_0 \frac{(1 - S_{11}^2 + S_{21}^2 - 2S_{12})}{(1 - S_{11})^2 - S_{21}^2}$$
(10)

where $Z_{\rm a}$, $R_{\rm a}$, $X_{\rm a}$, $Z_{\rm 0}$, and $S_{\rm ij}$ (i,j=1,2) indicate input impedance, input resistance, input reactance, characteristic impedance (50 Ω) of the VNA, and s-parameters. Using the input impedance measured at this stage, power reflection coefficient (Γ) is calculated from Eq. 1.

C. Read Range

Being a passive transponder, the Monza R6 chip in the Bellypatch is dependent on the energy wirelessly received from the interrogator. Read range is the maximum allowable Line of Sight (LOS) distance between the interrogator and the tag (Bellypatch). Maximum Effective Isotropic Radiated Power (EIRP) for the 902-928 MHz UHF RFID band is set to 36 dBm by the FCC [30]. In other words, the summation of input power (loss corrected) and antenna maximum gain should not exceed 36 dBm. We drive a 9 dBi maximum gain (G_a) commercial interrogator antenna [31] with a Speedway R420 reader unit [32] at 28 dBm input power ($P_{\rm in}$). Assuming 1 dB cable and connector loss ($P_{\rm loss}$), the maximum EIRP for the setup is 36 dBm ($P_{\rm in} + G_a - P_{\rm loss}$). We measure the read range of the Bellypatch antenna in a wide lab environment.

D. Bellypatch as a Respiration Monitor

We use the Bellypatch antenna on a SimBaby infant patient simulator mannequin [33] in a crib, and emulate a 20 breaths/minute breathing scenario (Fig. 14). A fabric belt is

TABLE I: Radiation efficiency of the Bellypatch antenna at 915 MHz

Antenna Orientation	Simulated Radiation Efficiency (%)	Measured Radiation Efficiency (%)
Relaxed and on-body (h = 11 mm)	45.1	43.1
Compressed and on-body (h = 6 mm)	29.0	26.9

used to ensure compression on the sensor. The Bellypatch is also placed on a male human subject, standing upright, to measure breathing activity. In both cases, the input power from the reader is 28 dBm, and the reader antenna gain is 9 dBi. 1 dB cable and connector loss is assumed.

VI. RESULTS AND DISCUSSION

A. Power Reflection Coefficient

Fig. 15 shows input resistance and reactance curves as a function of frequency, measured with the differential probe method. Fig. 16 shows the measured power reflection coefficient along with simulated results for different sizes (135 mm and 145 mm) of Bellypatch antennas in different orientations (free space, flat and on-body, bent). Compared to the 145 mm version, the 135 mm antenna has its resonant frequency closer to 900 MHz. The power reflection coefficient of the 135 mm version (free space, flat) ranges from -3 dB to -6 dB in the UHF RFID band (902 - 928 MHz). In the on-body-bent state, the resonant frequency gets higher, leading to higher reflection loss in the band of interest. Nevertheless, the antenna shows a good on-body read range. It is challenging to design an antenna that fits (in terms of Γ) all users in different age and body mass index (BMI) groups. By designing a more resilient antenna, it would be possible to exploit the full potential of the proposed design. On top of that, the "autotune" feature [6] is able to attain a better impedance match between the chip and the antenna, ensuring maximum power transfer.

B. Radiation Efficiency

Radiation efficiency is the ratio of the power radiated by the antenna to the power delivered to the antenna (after reflection) [34]. Measured on-body radiation efficiency of the antenna is 43.1% for h = 11 mm, and 26.9% for h = 6 mm. This reduction of radiation efficiency is responsible for lower RSSI when the antenna is compressed. Table I shows the simulated and measured on-body radiation efficiency of the Bellypatch.

C. Respiration Monitor

During inhalation, the expanding torso of the SimBaby exerts pressure on the Bellypatch, leading to reduced radiation efficiency. Consequently, sharp decline is observed in the backscattered power level (Fig. 18). In our experiment, the SimBaby is driven at a 20 breaths per minute rate. Fig. 18 shows 10 instances of sharp RSSI degradation. In other words,

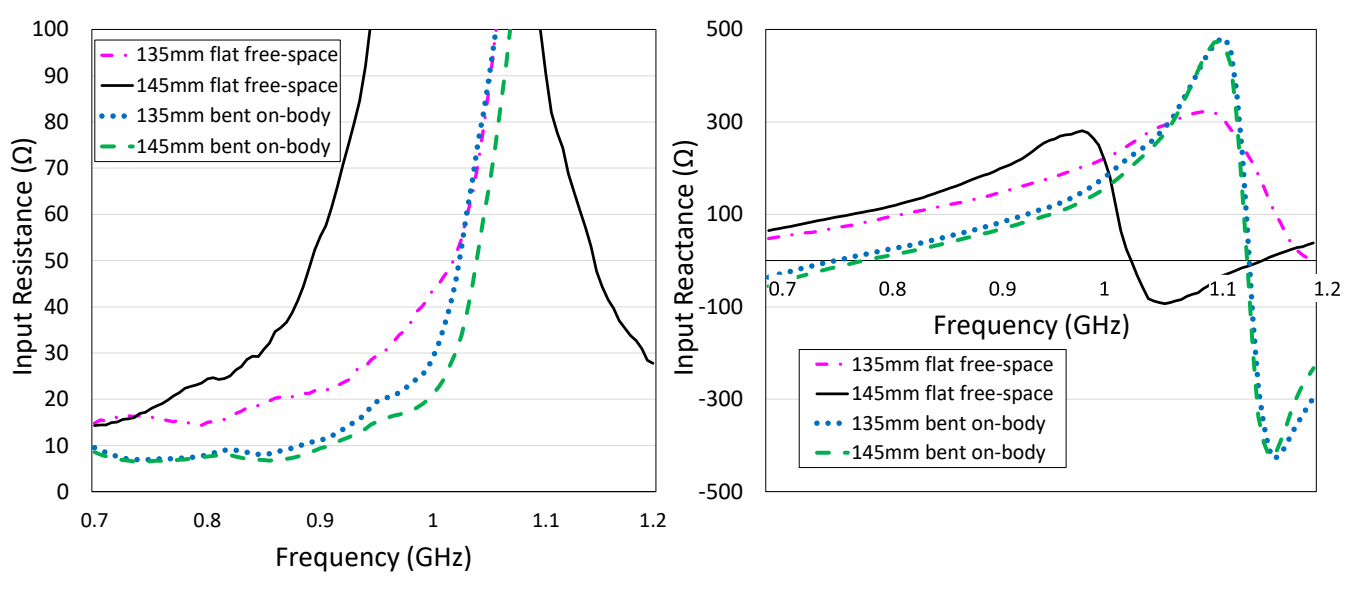


Fig. 15: Differential input resistance and reactance of the antennas in different orientations, measured with a differential probe.

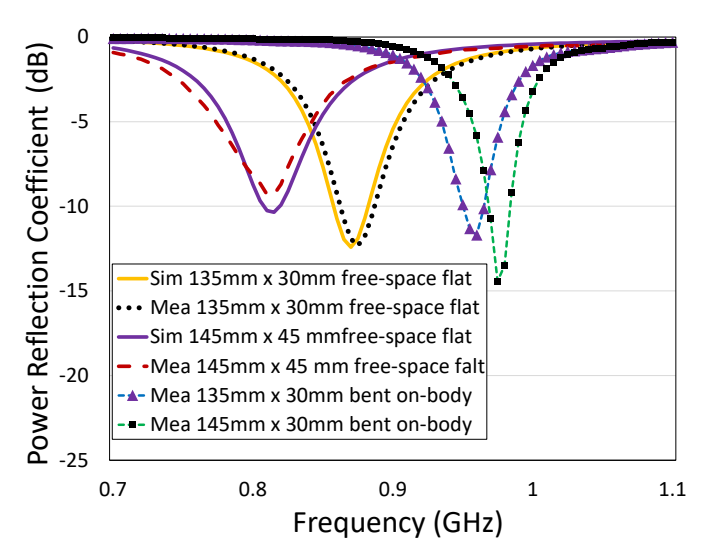


Fig. 16: Differential power reflection coefficients (Γ) of different Bellypatch samples.

the Bellypatch is successful in capturing 10 breathing cycles in 30 seconds. During on-body experimentation, the Bellypatch also successfully captured breathing instances (Fig. 19). The bellypatch captured 7 breathing instances in a 20 minutes window.

D. On-body Read Range

Fig. 17 shows the on-body RSSI readings from the 135 mm version of the Bellypatch as a function of the separation between the reader antenna and the Bellypatch. As the separation increases, the RSSI gets reduced, and the sensor gets out of monitoring beyond the separation of 4.1 m. In other words, the on-body read range of the 135 mm Bellypatch is 4.1 m. The read range of the larger version (145 mm) of the Bellypatch is 5.8 mm.

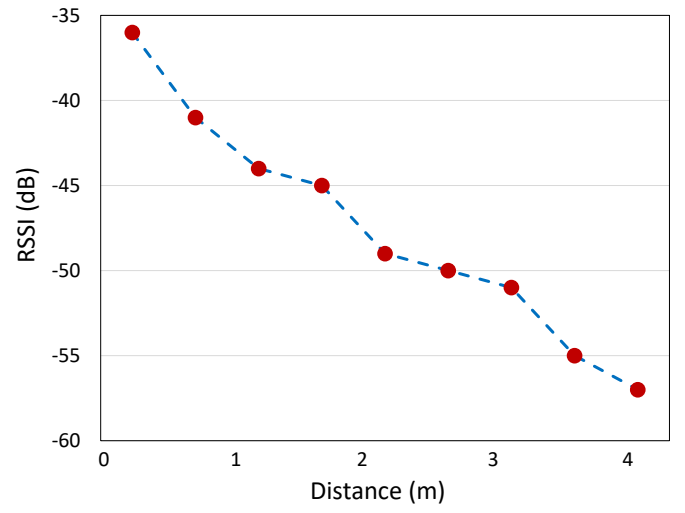


Fig. 17: RSSI vs distance between the reader and the belly-patch (on-body). The read range of the 135 mm \times 30 mm Bellypatch sample is 4.1 m.

The RSSI fluctuation from the successive compression and relaxation due to the breathing of the SimBaby mannequin causes sharp dips in the backscatter power level/RSSI received at the reader end (Fig. 18). The average power level during the relaxed state is -40 dBm. The maximum RSSI dip of 15 dB is observed in most cases. Unlike the SimBaby breathing scenario, the RSSI fluctuation in the human subject case (Fig. 19) is not regular, since a human breathing pattern is hard to precisely replicate. Nevertheless, the fluctuation in the RSSI level is clear. At least 6 dB fluctuation in the RSSI is observed between the 10th and 15th seconds. Due to the dynamic nature of the environment, machine learning algorithms can be used to determine the breathing rate and pattern from the RSSI data. The larger separation between the RSSI levels of two states (compressed and relaxed) facilitates the sensing information

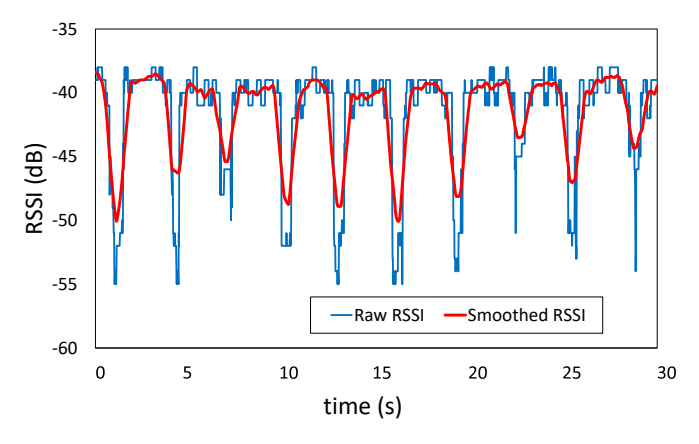


Fig. 18: Respiration monitoring (with the 135 mm band) RSSI data using a SimBaby mannequin emulating breathing at a 20 breaths/min rate.

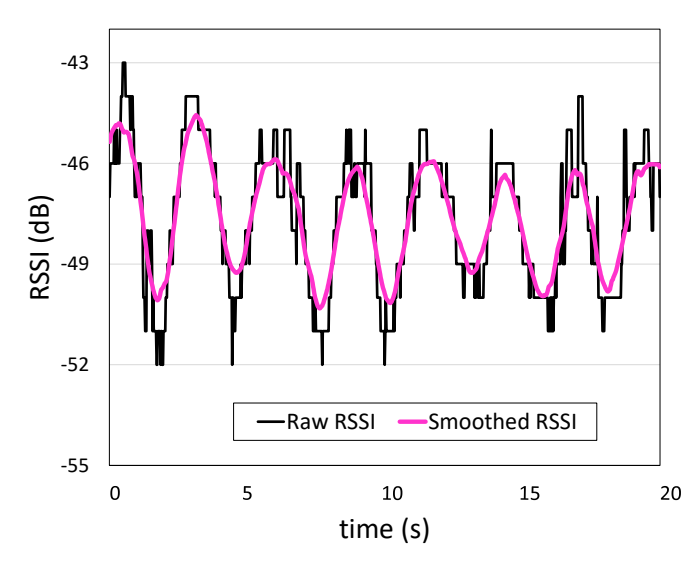


Fig. 19: Respiration monitoring (with the 135 mm band) RSSI with the Bellypatch placed around a human abdomen.

extraction procedure.

The maximum read range (5.8 m) of the sensor is justified using the using the following equation [4],

$$R = \frac{\lambda}{4\pi} antilog_{10} \left(\frac{-S + P_{in} + G_t + G_r - PLF}{20} \right)$$
 (11)

where S (dBm), $P_{\rm in}$ (27 dBm), $G_{\rm r}$, $G_{\rm t}$ (9 dBi), λ (0.328 m at 915 MHz), and PLF (3 dB for circular-linear polarization combination) are tag sensitivity (dBm), interrogator input power (dBm), receiver realized gain (dB), transmitter gain (dB), wavelength (meters), and polarization loss factor (dB) respectively. The cable (reader end) and metal-fabric connector (sensor end) loss are approximately 2 dB. From lab experiments, we find that the sensitivity (S) of Monza R6 chip is approximately -19 dBm. For the on-body bent Bellypatch, $G_{\rm r}=4.9$ dBi (maximum antenna gain) - 8.3 dB (loss due to impedance mismatch) - 1.5 dB (connector loss) = -4.9 dBi. Using equation 11, the predicted read range of the proposed Bellypatch is 5.9 m, which is close to the measured read range

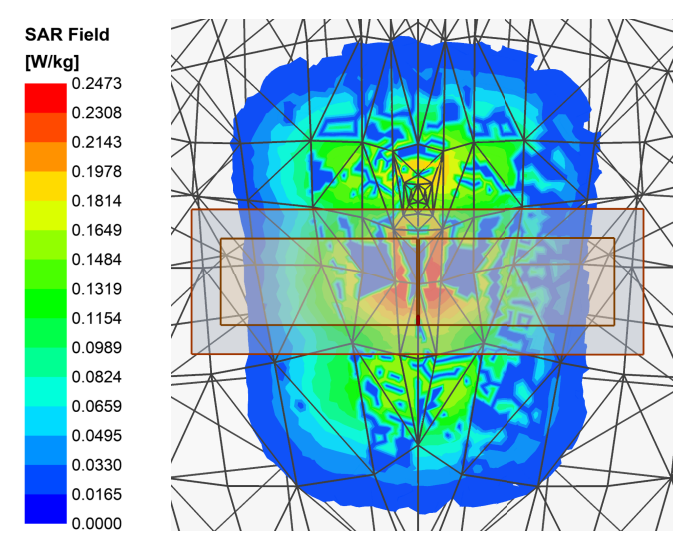


Fig. 20: Simulated SAR (Specific Absorption Rate) on the human torso. The maximum SAR is 0.2473 W/kg.

of 5.8 m. On the other hand, if the Bellyband (previous version with the Murata MAGICSTRAP chip [7]) is fabricated with a Monza R6 chip, the on-body read range would be 1.7 m. The variables associated with this calculation are as follows: $S = -19 \text{ dBm}, P_{in} = 27 \text{ dBm}, G_t = 9 \text{ dBi}, G_r = -13 \text{ dBi}$ (on-body gain) -0.96 dB (loss due to impedance mismatch) -1.5 dB (connector loss) = -15.5 dBi, PLF = 3 dB, and λ = 0.328 m. While it is true that the enhanced read range of the proposed Bellypatch antenna is partly due to the lower wake-up power of the Monza R6 chip, the read range is still 3.5-times greater than a Bellyband (previous version) made with a Monza R6 chip. Moreover, we can improve the antenna tuning by revising the design and examining on-body effects. If the power reflection coefficient of the proposed Bellypatch is -15 dB, the predicted read range is 15.1 m, under the abovementioned circumstances.

E. SAR and User Safety

Specific Absorption Rate (SAR) represents the dielectric heating due to radiation. If the input power from a reader is 27 dBm, transmitter gain 9 dBi, distance 1 m, receiver gain 5 dBi, maximum received power by the antenna is 9.3 dBm or 8.53 mW. If we assume zero power consumption by the chip, the maximum SAR on the human body is 0.247 W/kg (Fig. 20), lower than the maximum allowable value 1.6 W/kg [35].

The proposed Bellypatch antenna shows significant improvement compared to the Bellyband [2, 3]. Table II shows a comparison between the two antennas.

VII. CONCLUSION

We propose a wearable, battery-less, knitted compression sensing antenna (Bellypatch) and show its use as an onbody respiration monitor. The proposed sensor is a patch type antenna with a flexible polyethylene foam substrate. Because of its patch structure, the antenna is capable of retaining

TABLE II: Comparison between the Bellyband [3] and the proposed Bellypatch antennas

	Bellyband [2,3]	Bellypatch (Proposed)
Sensing property	Strain	Compression
RFID chip	Murata Magicstrap [2]	Monza R6 [5]
Dimensions (mm ³)	Relaxed: $81 \times 20 \times 1$, Stretched: $100 \times 20 \times 1$	Relaxed: 135×30×11, Compressed: 135×30×6
Chip Input Impedance	25 - j200 Ω	12 - j120 Ω
Maximum radiation efficiency (on-body)	7.3% [4]	43.1%
Read range (on-body)	0.6 m	4.1 m (135 mm band), 5.8 m (145 mm band)
Radiation pattern	Omnidirectional	Directional

radiation efficiency in the proximity of the human body, unlike the dipole antenna family of strain sensors. The antenna not only shows good on-body radiation efficiency (43.1%) but also shows good sensitivity in response to compression. As the antenna is compressed, the radiation efficiency gets reduced, leading to a lower backscatter power level (RSSI) at the reader. The maximum on-body read range of the proposed antenna is 5.8 m. The proposed antenna is reusable. The Bellypatch is larger in size (135 mm \times 30 mm \times 11mm) compared to the folded dipole Bellyband (100 mm \times 20 mm \times 1 mm). However, the on-body performance justifies the size. In future work, we will demonstrate a miniaturization process for the Bellypatch antenna. Furthermore, machine learning techniques will be used for estimating breathing rate and actuating a ventilator. The sensor can also be used for monitoring uterine activity during pregnancy, body movement, and general on-body tracking applications. We will also investigate the Bellypatch antenna performance by fabricating the antenna with lower-conductivity materials to improve the bandwidth. Low-conductivity materials can increase antenna bandwidth by increasing loss and reducing the quality factor. Although low-conductivity material would lead to reduced antenna gain, we will seek to optimize the antenna design so that we get the maximum possible read range that would lie between the current maximum read range (5.8 m) and the predicted maximum possible range (15.1 m).

REFERENCES

- G. Marrocco, "Gain-optimized self-resonant meander line antennas for RFID applications," *IEEE Antennas and Wireless Propagation Letters*, vol. 2, pp. 302–305, 2003.
- [2] D. Patron, W. Mongan, T. P. Kurzweg, A. Fontecchio, G. Dion, E. K. Anday, and K. R. Dandekar, "On the Use of Knitted Antennas and Inductively Coupled RFID Tags for Wearable Applications," *IEEE Transactions on Biomedical Circuits and Systems*, vol. 10, no. 6, pp. 1047–1057, 2016.
- [3] Y. Liu, A. Levitt, C. Kara, C. Sahin, G. Dion, and K. R. Dandekar, "An improved design of wearable strain sensor based on knitted RFID

- technology," in 2016 IEEE Conference on Antenna Measurements Applications (CAMA), 2016, pp. 1–4.
- [4] M. A. S. Tajin, O. Bshara, Y. Liu, A. Levitt, G. Dion, and K. R. Dandekar, "Efficiency measurement of the flexible on-body antenna at varying levels of stretch in a reverberation chamber," *IET Microwaves, Antennas Propagation*, Jul 2019.
- [5] "Monza R6 Chip Datasheet [Online]," https://support.impinj.com/hc/enus/articles/115001376564-Monza-R6-A-Product-Brief-Datasheet, accessed: 2020-08-24.
- [6] "Monza R6 AutoTune [Online]," www.support.impinj.com/hc/enus/articles/202356796-AutoTune-Technology-White-Paper/, accessed: 2020-07-30.
- [7] "Murata MAGICSTRAP UHF RFID Tag [Online]," https://laerdal.com/ us/Simbaby/, accessed: 2020-11-01.
- [8] M. A. S. Tajin, A. S. Levitt, Y. Liu, C. E. Amanatides, C. L. Schauer, G. Dion, and K. R. Dandekar, "On the effect of sweat on sheet resistance of knitted conductive yarns in wearable antenna design," *IEEE Antennas* and Wireless Propagation Letters, vol. 19, no. 4, pp. 542–546, 2020.
- [9] U. Tata, H. Huang, R. L. Carter, and J. C. Chiao, "Exploiting a patch antenna for strain measurements," *Measurement Science and Technology*, vol. 20, no. 1, p. 015201, nov 2008. [Online]. Available: https://doi.org/10.1088%2F0957-0233%2F20%2F1%2F015201
- [10] A. Daliri, A. Galehdar, J. Sabu, W. Rowe, and K. Ghorbani, "Circular microstrip patch antenna strain sensor for wireless structural health monitoring," in WCE 2010, 2010.
- [11] C. Occhiuzzi, C. Paggi, and G. Marrocco, "Passive RFID strain-sensor based on meander-line antennas," *IEEE Transactions on Antennas and Propagation*, vol. 59, no. 12, pp. 4836–4840, 2011.
- [12] S. Merilampi, T. Bjorninen, L. Ukkonen, P. Ruuskanen, and L. Sydanheimo, "Embedded wireless strain sensors based on printed RFID tag," *Sensor Review*, vol. 31, pp. 32–40, 2011.
- [13] Feiyuan Long, Xiao Dong Zhang, T. Björninen, J. Virkki, L. Sydänheimo, Yan-Cheong Chan, and L. Ukkonen, "Implementation and wireless readout of passive UHF RFID strain sensor tags based on electro-textile antennas," in 2015 9th European Conference on Antennas and Propagation (EuCAP), 2015, pp. 1–5.
- [14] T. Koskinen and Y. Rahmat-Samii, "Metal-mountable microstrip RFID tag antenna for high impedance microchip," Eur. Conf. Antennas Propagation, EuCAP 2009, Proc., pp. 2791–2795, 2009.
- [15] K. Lin, S. Chen, and R. Mittra, "A looped-bowtie RFID tag antenna design for metallic objects," *IEEE Transactions on Antennas and Prop*agation, vol. 61, no. 2, pp. 499–505, 2013.
- [16] H. Rajagopalan and Y. Rahmat-Samii, "Conformal RFID antenna design suitable for human monitoring and metallic platforms," in *Proceedings* of the Fourth European Conference on Antennas and Propagation, 2010, pp. 1–5.
- [17] A. Dubok and A. B. Smolders, "Miniaturization of robust UHF RFID antennas for use on perishable goods and human bodies," *IEEE Antennas* and Wireless Propagation Letters, vol. 13, pp. 1321–1324, 2014.
- [18] A. P. Sohrab, Y. Huang, M. N. Hussein, and P. Carter, "A hybrid UHF RFID tag robust to host material," *IEEE Journal of Radio Frequency Identification*, vol. 1, no. 2, pp. 163–169, 2017.
- [19] "FCC Guidelines for Human Exposure Exposure to RF Fields [Online]," https://transition.fcc.gov/bureaus/oet/info/documents/bulletins/oet65/ oet65b.pdf, accessed: 2020-08-25.
- [20] C. Luo, I. Gil, and R. Fernández-García, "Wearable textile UHF-RFID sensors: A systematic review," *Materials (Basel)*., vol. 13, no. 15, aug 2020.
- [21] P. Sen, S. N. R. Kantareddy, R. Bhattacharyya, S. E. Sarma, and J. E. Siegel, "Low-Cost Diaper Wetness Detection Using Hydrogel-Based RFID Tags," *IEEE Sens. J.*, vol. 20, no. 6, pp. 3293–3302, 2020.
- [22] M. A. S. Tajin, W. M. Mongan, and K. R. Dandekar, "Passive rfid-based diaper moisture sensor," *IEEE Sensors Journal*, vol. 21, no. 2, pp. 1665–1674, 2021.
- [23] P. Lugoda, J. C. Costa, C. Oliveira, L. A. Garcia-Garcia, S. D. Wickramasinghe, A. Pouryazdan, D. Roggen, T. Dias, and N. Münzenrieder, "Flexible temperature sensor integration into e-textiles using different industrial yarn fabrication processes," Sensors, vol. 20, no. 1, 2020. [Online]. Available: https://www.mdpi.com/1424-8220/20/1/73
- [24] M. Han, Y. Liu, R. Rakhmanov, C. Israel, M. A. S. Tajin, G. Friedman, V. Volman, A. Hoorfar, K. R. Dandekar, and Y. Gogotsi, "Solution-Processed Ti3C2Tx MXene Antennas for Radio-Frequency Communication," Adv. Mater., vol. 2003225, pp. 1–7, 2020.
- [25] M. Yu, G. Yu, and B. Dai, "Graphene fiber-based strain-insensitive wearable temperature sensor," *IEEE Sensors Letters*, vol. 4, no. 10, pp. 1–4, 2020.

- [26] S. Uzun, M. Han, C. J. Strobel, K. Hantanasirisakul, A. Goad, G. Dion, and Y. Gogotsi, "Highly conductive and scalable ti3c2tx-coated fabrics for efficient electromagnetic interference shielding," *Carbon*, 2020. [Online]. Available: http://www.sciencedirect.com/science/article/pii/S0008622320311982
- [27] T. Delipinar, E. A. Ozek, C. E. Kaya, S. Tanyeli, and M. K. Yapici, "Flexible graphene textile rfid tags based on spray, dispense and contact printing," in 2020 IEEE International Conference on Flexible and Printable Sensors and Systems (FLEPS), 2020, pp. 1–4.
- [28] R. Papazyan, P. Pettersson, H. Edin, R. Eriksson, and U. Gäfvert, "Extraction of high frequency power cable characteristics from Sparameter measurements," *IEEE Transactions on Dielectrics and Elec*trical Insulation, vol. 11, no. 3, pp. 461–470, 2004.
- [29] I. Kiirgad, S. Member, N. Dagli, G. L. Matthaei, L. Fellow, S. I. Long, and S. Member, "Experimental Analysis of Transmission Line Parameters in High-speed GaAs Digital Circuit Interconnects," vol. 39, no. 8, 1991.
- [30] "FCC Electronic Code of Federal Regulations [Online]," https://www.ecfr.gov/cgi-bin/text-idx?SID=eed706a2c49fd9271106c3228b0615f3&mc=true&node=pt47.1.15&rgn=div5, section: 15.247, Accessed: 2020-04-08.
- [31] "Circular Polarity RFID Panel Antenna [Online]," http://assets.lairdtech. com/home/brandworld/files/ANT-DS-S9028PCL%20S9028PCR-0515.pdf/, accessed: 2020-05-17.
- [32] "Speedway Reader Datasheet [Online]," https://support.impinj.com/ hc/en-us/articles/202755388-Impinj-Speedway-RAIN-RFID-Reader-Family-Product-Brief-Datasheet/, accessed: 2020-08-24.
- [33] "Laerdal SimBaby Infant Patient Simulator [Online]," https://laerdal.com/us/Simbaby/, accessed: 2020-11-01.
- [34] C. A. Balanis, Antenna theory: analysis and design, 2005, pp. 85-86.
- [35] "Specific Absorption Rate (SAR) for Cellular Telephones [Online]," https://www.fcc.gov/consumers/guides/wireless-devices-and-health-concerns, accessed: 2020-08-24.